Data-Based Resilience Enhancement Strategies for Electric-Gas Systems Against Sequential Extreme Weather Events

Rong-Peng Liu, *Graduate Student Member, IEEE*, Shunbo Lei, *Member, IEEE*, Chaoyi Peng, *Member, IEEE*, Wei Sun, *Member, IEEE*, and Yunhe Hou, *Senior Member, IEEE*

***Abstract*—Some extreme weather events, such as the hurricane, pass through an area sequentially and thus are called sequential extreme weather events (SEWEs). This paper proposes a data-based robust optimization (RO) model to enhance the resilience of the integrated electricity and gas system (IEGS) against SEWEs. Specifically, the SEWE strikes the IEGS sequentially. After each attack, the system state is adjusted immediately to minimize the maximized expected system cost caused by the SEWE. The attack-defense procedures are repeated alternatively during the SEWE. Preventive measures, hardening, are made in advance to reduce the impact of sequential attacks. The entire process is formulated as a multi-period RO model. It is proved that the most effective resilience enhancement strategies for this model are the same as those for a two-stage RO model, which can be solved by the nested column-and-constraint generation (C&CG) algorithm. In addition, the property of SEWEs, sequentially endangering limited regions of the IEGS, is incorporated to build a data-based uncertainty set and reduce its conservativeness. Simulation results on two IEGSs validate the effectiveness of the proposed model.**

***Index Terms*—Integrated electricity and gas systems, mixed-integer programming, resilience, robust optimization.**

Manuscript received October 31, 2019; revised February 18, 2020 and May 22, 2020; accepted June 20, 2020. Date of publication July 7, 2020; date of current version October 21, 2020. The work of Rong-Peng Liu, Shunbo Lei, Chaoyi Peng, and Yunhe Hou was supported in part by the National Natural Science Foundation of China under Grant 51677160, in part by the Research Grants Council of Hong Kong under Grant GRF17207818, and in part by the Research Grants Council of Hong Kong through the Theme-Based Research Scheme under Project T23-701/14-N. The work of Wei Sun was supported in part by the U.S., National Science Foundation under Grant ECCS-1552073, and in part by the U.S., Department of Energy under Award DE-EE0007998. Paper no. TSG-01658-2019. *(Corresponding author: Shunbo Lei.)*

Rong-Peng Liu is with the Department of Electrical and Electronic Engineering, University of Hong Kong, Hong Kong (e-mail: rpliu@eee.hku.hk).

Shunbo Lei was with the University of Hong Kong, Hong Kong. He is now with the Department of Electrical Engineering and Computer Science, University of Michigan, Ann Arbor, MI 48109 USA (e-mail: shunbol@umich.edu).

Chaoyi Peng is with the Power Dispatch and Control Center, China Southern Power Grid Company Ltd., Guangzhou 510623, China (e-mail: pcychopin@gmail.com).

Wei Sun is with the Department of Electrical and Computer Engineering, University of Central Florida, Orlando, FL 32186 USA (e-mail: sun@ucf.edu).

Yunhe Hou is with the Department of Electrical and Electronic Engineering, University of Hong Kong, Hong Kong, and also with the Shenzhen Institute of Research and Innovation, University of Hong Kong, Shenzhen 518057, China (e-mail: yhhou@eee.hku.hk).

Color versions of one or more of the figures in this article are available online at http://ieeexplore.ieee.org.

Digital Object Identifier 10.1109/TSG.2020.3007479

NOMENCLATURE

Sets

$\mathcal{D}^p/\mathcal{D}^g$	Set of loads in power/gas network.
$\mathcal{G}^p/\mathcal{G}^g$	Set of traditional (coal-fired)/gas-fired units.
$\mathcal{L}^p/\mathcal{L}^g/\mathcal{C}^g$	Set of power transmission lines/gas passive pipelines/gas compressors (gas active pipelines).
$\mathcal{N}^p/\mathcal{N}^g$	Set of nodes in power/gas network.
$\mathcal{S}$	Set of gas storage facilities.
$\mathcal{T}$	Set of time steps during the unfolding processes, i.e., $\{1,\ldots,T\}$.
$\mathcal{U}^t$	Set of regions at time t.
$\mathcal{W}$	Set of gas wells.
$[M]$	Set of integers from 1 to M, i.e., $\{1, 2,\ldots, M\}$.

Parameters

$\mathrm{E}_{\mathrm{total}}$	Budget of preventive measures.
$\mathrm{C}_{dp}/\mathrm{C}_{dg}$	Cost of load shedding in power/gas network.
$\mathrm{C}_p(\cdot)$	Cost function of traditional unit.
C_w	Cost of gas well output.
$\mathrm{G}_g^d/\mathrm{G}_g^u$	Ramp down/up limit of gas-fired unit.
$\mathrm{G}_g^{\min}/\mathrm{G}_g^{\max}$	Output limits of gas-fired unit.
$\mathrm{G}_i^{\min}/\mathrm{G}_i^{\max}$	Limits of pressure square in gas network.
$\mathrm{G}_s^{\mathrm{in}}/\mathrm{G}_s^{\mathrm{out}}$	Input/output limit of gas storage facility.
$\mathrm{G}_s^{\max}$	Volume of gas storage facility.
$\mathrm{G}_w^{\max}$	Output limit of gas well.
M	The number of segments in gas passive pipeline.
$\mathrm{P}_d/\mathrm{G}_d$	Load in power/gas network.
$\mathrm{P}_g^{\mathrm{d}}/\mathrm{P}_g^{\mathrm{u}}$	Ramp down/up limit of traditional unit.
$\mathrm{P}_g^{\min}/\mathrm{P}_g^{\max}$	Output limits of traditional unit.
$\mathrm{P}_l/\mathrm{G}_l/\mathrm{G}_c$	Transmission limit of power transmission line/gas passive pipeline/gas compressor.
W_l	Weymouth equation constant.
x_l	Reactance of power transmission line.
α_c	Gas compressor constant.
$\theta_i^{\max}$	Limit of phase angle in power network.

Variables

e_l/e_w	Binary variable, 1 represents the corresponding power transmission line/gas well is protected, and 0 otherwise.

f_l^t/f_w^t	Binary variable, 1 represents the power transmission line /gas well is attacked at time t, and 0 otherwise.
$g_{\text{in},s}^t/g_{\text{in},s}^t$	Input/output of gas storage facility at time t.
g_s^t	Gas stored in gas storage facility at time t.
g_w^t	Output of gas well at time t.
p_d^t/g_d^t	Load shedding in power/gas network at time t.
p_g^t/g_g^t	Output of traditional/gas-fired unit at time t.
$p_l^t/g_l^t/g_c^t$	Power/gas/gas flow through power transmission line/gas passive pipeline/gas compressor at time t.
$p_{r_t,r_{t-1}}^t$	Probability of region r_t being attacked at time t conditioning that region r_{t-1} has been attacked at time $t-1$.
u_g^t	Binary variable, 1 represents the generator is running at time t, and 0 otherwise.
θ_i^t/π_i^t	Phase angle/pressure square at time t.

I. Introduction

COMPARED with traditional power generation technology, the gas-fired generation receives more attention for its superior characteristics, such as low pollution, fast response, and high efficiency. Moreover, the breakthrough in natural gas extraction techniques stimulated the drop in gas prices and prospered its development [1]. Now, natural gas has become one of the dominant energy resources to generate power in some countries, e.g., the U.S. [2] and the U.K. [3]. However, the integrated electricity and gas system (IEGS) faces more security and reliability related challenges [4]–[9] due to complex coupling relations [10] and attracts many researchers. Reference [4] proposes a security-constrained optimal power and gas flow model to conduct security analysis. A security-constrained expansion planning model is proposed for the IEGS in [5] to check $N-1$ contingencies. Reference [6] characterizes the robust security region for the IEGS and guarantees the security of the operation strategy. Reference [7] presents a reliability-based economic expansion planning model for energy hubs. In [8], a robust economic expansion planning model for the IEGS is proposed to minimize the sum of the investment and operation cost. Meanwhile, its optimal solution also satisfies both $N-1$ and probabilistic reliability criteria. Reference [9] proposes a universal generating function technique-based multi-state model to evaluate the reliability of the IEGS.

In addition, the number of extreme weather events is increasing due to global warming [11], which even exacerbates the above challenges. For example, Hurricane Sandy, one of the most devastating natural disasters, led to the outages of power transmission lines and influenced more than 8 million people in America [12]. According to [10], a tornado resulted in the loss of load in an Australian IEGS in 2016. Deliberate human attacks are another kind of threat to the IEGS [13]. Resilience enhancement strategies are effective in reducing the impact of these extreme events. The resilience of a system refers to its capability to mitigate the duration and/or the magnitude of high-impact low-frequency extreme events [14]. Different resilience enhancement strategies are implemented [15]–[30] according to the stages of extreme events.

Before extreme events, preventive measures are effective. Specifically, stochastic programming and robust optimization (RO) based IEGS expansion planning methods are introduced in [15] and [16], respectively, to enhance the resilience of the IEGS. System expansion usually aims at long-term profits and is time-consuming (from months to years). In addition, the component hardening is quite effective in constructing resilient IEGS against extreme events [17], [18]. Generally, hardening is faster than expansion (several days). Proactive scheduling [19] is also included in this time scale. Other preventive measures, e.g., mobile emergency generators [20] and unit commitment [21], [22], are proposed to address extreme events (from minutes to hours).

After extreme events, system restoration has a high priority. New restoration strategies are indispensable, as outages caused by extreme events have some new features [23], e.g., prolonged outage duration and extended outage scale. A graph theory-based restoration method is proposed to speed up the process of system recovery in [24]. Reference [25] restores the critical loads by dividing the distribution system into multiple microgrids and powering them with distributed generators. In [26], a distributed method is implemented to detect faults and restore critical loads. Reference [27] proposes a repair crew dispatch method to construct resilient IEGS and thus reduces the post-event repair duration.

During extreme events (also called the *unfolding process*), only a small number of actions can be taken due to the limited response time. Assuming the track of extreme weather events is predictable, reference [28] models the unfolding process as a Markov process, and the optimal power re-dispatch decisions are obtained by solving a stochastic optimization model. An RO model is proposed in [29] to enhance system resilience, provided the track of the natural disaster is stochastic within a range. Reference [30] introduces a self-healing resilience system, where the power system is sectionalized into one main grid and several microgrids to maximize power supply when some transmission lines are broken. However, the influence of extreme weather events on the IEGS during the unfolding process is not considered in the previous work. In fact, the components that could be destroyed by extreme weather events in power and gas networks are quite different (see Section II for details). Moreover, the failure in one network may completely change the operation state of the other, due to the complex coupling relations. The resilience of the IEGS during extreme weather events should be highly regarded.

Some extreme weather events, e.g., hurricanes and tornadoes, pass through an area *sequentially and regionally* and thus are called sequential extreme weather events (SEWEs). In this paper, their unique sequential and regional property is designated as the *Markov property* (see Section II-A for details). We focus on the impact of SEWEs on the IEGS, as they cause a large volume of power outages among all extreme events. The strategies, components hardening before SEWEs and system re-dispatch during SEWEs, are proposed to enhance the system resilience. The contributions are twofold:

1) Resilience enhancement strategies for IEGSs before and during SEWEs. The SEWE strikes the IEGS sequentially. After each attack, system operators strive to minimize the maximized expected system cost caused by the SEWE using system re-dispatch. The attack-defense procedures are implemented alternatively during the SEWE. Preventive measures, hardening, are made in advance to reduce the impact of sequential attacks. The entire process is formulated as a multi-period RO model. It is proved that the most effective resilience enhancement strategies for this model are the same as those for a two-stage RO model, which is solved by the nested column-and-constraint generation (nested C&CG) algorithm.

2) Data-based uncertainty set. According to the historical or forecast data, the direction, range, and intensity of an SEWE are estimated. This indicates that the SEWE cannot reach some regions in the IEGS within a limited period. Thus, the combinations of system components that may suffer from the strike of the SEWE are reduced, which is equivalent to cutting down the number of scenarios in the uncertainty set and leads to a less conservative RO model. Simulation results validate the effectiveness of the proposed model in enhancing the resilience of the IEGS. In addition, the data-based uncertainty set also contributes to the improvement in computational efficiency.

Compared with [29], this work incorporates the natural gas network. Different from [18], the influence of the SEWE on the IEGS is investigated. Different from [17] and other previous work, based on historical or forecast data, we consider the influence of the sequential and regional property, i.e., the Markov property, of the SEWE on the IEGS and utilize this property to reduce the conservativeness of the uncertainty set.

The rest of this paper is organized as follows. Section II introduces the Markov property of SEWEs and the data-based method. The proposed RO model is presented in Section III. Section IV derives the solution method. Simulation results are displayed in Section V. Section VI concludes this paper.

II. Property of SEWEs and Data-Based Method

As one of the most common SEWEs [31]–[33], the hurricane is selected as the representative of SEWEs. The influence of other SEWEs on the IEGS can be analyzed similarly. Firstly, we make the following assumptions and simplifications.

1) The steady state is considered after each attack [15]–[18]. The transient state is another important research topic but beyond the scope of this paper.
2) Power transmission lines and gas wells suffer from hurricane strikes. It is reasonable as power transmission lines are in the air, and many gas wells are on the sea without any protection. Other components, e.g., underground gas pipelines and power units (usually in power plants), cannot be easily destroyed by a hurricane [22].
3) Components will not be affected by a hurricane if they are hardened in advance [17], [18], [29]. Practical hardening measures include: i) building wind barriers (for gas wells); ii) reducing the span length, building guy wires, and underground-ing (for power transmission lines) [17], [18].
4) Components are attacked at discrete time t, $t \in [T]$, followed by re-dispatch decisions. This assumption is valid to simplify the model with promising accuracy [28], [29].

Meanwhile, some phrases are explained as follows.

1) Hereinafter, "preventive measures" denote the hardening measures which are taken to protect power transmission lines and gas wells before the hurricane.
2) "System cost" denotes the sum of the operation cost arising from: i) the outputs of power generators and gas wells, and ii) the penalty of the power and gas load shedding.
3) "Investment cost" denotes the cost arising from preventive measures.
4) "Total cost" denotes the sum of the cost arising from: i) the system cost, and ii) the investment cost.

A. Sequential and Regional Property of a Hurricane

In this paper, the direction, range, and intensity of a hurricane are leveraged to estimate its track passing through an IEGS. Different from some extreme events, the hurricane endangers the entire IEGS sequentially. Since the hurricane intensity cannot be arbitrarily large, only the regions near the hurricane center can be reached sequentially. Namely, only components near the hurricane center may suffer from the strike sequentially. The sequential and regional property is called the *Markov property*. An illustrative example is shown in Fig. 1.

The system is divided into four regions. Solid lines are power transmission lines or gas pipelines, and circles are power buses or gas nodes. Considering the *Markov property*, it is assumed that the hurricane only influences the neighboring regions as well as the same region at the next time step. For example, if line 1 in Region 1 is destroyed at $t = 1$, lines 2 and 3 in Regions 1 and 2 may suffer from the hurricane strike at $t = 2$. However, line 4 in Region 3 will not be affected. Region 1 is called the same region, and Region 2 is called the neighboring region. According to this property, the data-based uncertainty set is constructed (see Section III-C for details). It is easy to figure out that the direction and the range of a hurricane and the region partition of an IEGS are significant for the proposed uncertainty set and heavily rely on data. Thanks to an extreme volume of historical data about the hurricane and the improvement of forecast technique [31]–[33], data-based methods, introduced in the next subsection, are quite applicable.

B. Data-Based Method

To obtain the direction and range of a hurricane and the region partition of an IEGS, this subsection introduces two types of data-based methods for different purposes.

Based on the *historical hurricane data* (direction, intensity, etc.) on a hurricane-prone area, the *preventive hardening*, which can be implemented at any time, is taken to protect critical components in the local IEGS against *future hurricanes*. According to [31], from 1851 to 2018, Florida (120), Texas (64), North Carolina (56), and Louisiana (54) are the

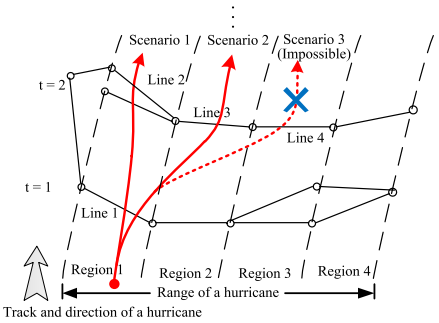

Fig. 1. Explanation of the Markov property.

top four hurricane-prone states in the U.S., and major hurricanes mostly appeared in Florida (34), Texas (19), and Louisiana (17), i.e., the Gulf Coast of the U.S. Thus, historical hurricane data on the Gulf Coast (from 1851 to 2018) is analyzed and utilized to help to obtain an estimated hurricane model. Details are as follows.

1) Overall direction. According to [31], the most common hurricane direction of a state is obtained and is utilized as the overall direction. For example, in Texas, nearly all hurricanes are southwesterly, and the southerly hurricanes overwhelm the others in Louisiana. Note that local direction changes are allowed, provided the overall direction keeps unchanged, e.g., Scenario 2 in Fig. 1.
2) Range of a hurricane. In order to obtain the most critical components in the IEGS, the range of the hurricane is assumed to incorporate the entire IEGS. Besides, according to [31], landing locations of historical hurricanes are dispersive. Given the overall hurricane direction, it is assumed the hurricane can land at any location of the IEGS in the beginning. For example, in Fig. 1, any one of the regions (Region 1 to Region 4) in the beginning ($t = 1$) may suffer from the hurricane strike. It is the range and unfixed landing location that ensure the optimality of the critical components obtained by the proposed model (see Section III for details).
3) Intensity. According to [31], hurricane intensities vary from states to states (shown in Table I). Category 1 hurricanes are not incorporated, as they cause little damage to the IEGS. Specifically, in Florida (FL) and Texas (TX), Categories 2 to 4 hurricanes are considered. Louisiana (LA), Mississippi (MS), and Alabama (AL) need to protect local IEGSs from Category 2 and 3 hurricane strikes. Based on the number of appearances, the *weighted mean of the dominating hurricane Categories* is leveraged to implement the region partition. For example, the hurricane intensity utilized for the region partition in LA is 181 km/h. According to the intensity and the range of a hurricane, the region partition is obtained. For example, if the range of an IEGS is 720 km and the hurricane intensity is 180 km per unit time, this IEGS is divided into four regions (see Fig. 1).

In addition, based on *hurricane track and intensity forecast data*, the *emergency hardening* is taken to protect the critical components in the local IEGS against a *specific upcoming hurricane* and should be finished before its arrival. According to the state-of-the-art hurricane forecast technique [31], the average hurricane track and intensity forecast errors in 2018, presented in Table II, are utilized to help to obtain an estimated hurricane model. Details are as follows.

1) Overall direction. Due to the promising accuracy [31], the forecasted direction of an upcoming hurricane is directly used.
2) Range of a hurricane. Existing forecast methods cannot provide an accurate hurricane track [31]–[33]. Instead, we resort to a rational range of the hurricane track. According to the hurricane track forecast error (shown in Table II) and the forecasted track, the range of the hurricane track is estimated. An example is shown in Fig. 2.
3) Intensity. According to the definition of a hurricane, its intensity is larger than or equal to 119 km/h. Compared with the forecasted hurricane intensity and the track error, the intensity error is small. Thus, the forecasted hurricane intensity can be directly used for the region partition.

TABLE I
HURRICANE CATEGORIES OF GULF STATES

Category	Intensity (km/h)	FL	TX	LA	MS	AL
2	154-177	36	16	14	6	5
3	178-208	24	12	14	7	5
4	209-251	11	7	2	0	0
5	>251	2	0	1	1	0

TABLE II
FORECAST ERROR

Forecast horizon (h)	12	24	36	48	72	96	120
Track error (km)	37.5	56	73.1	99.0	164.2	238.2	307.9
Intensity error (km/h)	9.1	14.4	17.0	18.9	23.4	23.7	22.6

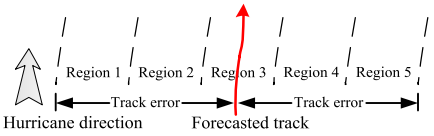

Fig. 2. Range of a hurricane.

III. PROBLEM FORMULATION

A. Objective Function

The hurricane strikes the component in one of the regions at time t, $t \in [T]$, followed by system re-dispatch after each attack immediately to minimize the maximized expected system cost caused by the hurricane under operation constraints. Preventive measures, hardening, are made in advance to protect critical components and reduce the expected system cost. The entire process is formulated as the *tri-level* optimization problem (1).

$$\phi'_T(\mathbf{e},\mathbf{p},\mathbf{a}) = \min_{\mathbf{e}\in\mathcal{E}}\left\{\max_{\mathbf{p}\in\Delta}\left\{\min_{\mathbf{a}\in\mathcal{A}(\mathbf{e},\mathbf{p})}\left(\sum_{t=1}^{T}\mathbf{E}[c(\mathbf{a}_t)]\right)\right\}\right\}. \quad (1)$$

The upper level variable $\mathbf{e}$ consists of preventive measures e_l and e_w. $\mathbf{p}$ is the middle level random variable and is composed of $p^t_{r_t,r_{t-1}}$. Since we do not know the distribution of $\mathbf{p}$, only two constraints are inferred: i) $0 \le p^t_{r_t,r_{t-1}} \le 1$ and ii) $\mathbf{1}^{\mathrm{T}} \cdot \mathbf{p}^t_{r_{t-1}} = 1$. $\mathbf{p}^t_{r_{t-1}} = col(p^t_{1,r_{t-1}}, \ldots, p^t_{R_t,r_{t-1}})$ and R_t is the number of regions at time t. For example, there are 4 partitioned regions at $t = 2$ in Fig. 1, so $R_2 = 4$. $\mathbf{a}$, $\mathbf{a} = col(\mathbf{a}_1, \ldots, \mathbf{a}_T)$, represents variables in the lower level. $\mathcal{E}$, Δ, and $\mathcal{A}$ are feasible regions. $c(\mathbf{a}_t)$, $c(\mathbf{a}_t) = \sum_g C_p(p^t_g) + \sum_w C_w \cdot g^t_w + \sum_d C_{dp} \cdot p^t_d + \sum_d C_{dg} \cdot g^t_d$, is the cost at time t. $\mathrm{C}_p(\cdot)$ is a positive semi-definite quadratic function and is linearized by piecewise linear methods [34]. Solving problem (1) directly is computationally intractable due to the nonconvex objective function, even if its feasible region is convex. Instead, we consider the problem (2).

$$\phi_T(\mathbf{e},\mathbf{f},\mathbf{a}) = \min_{\mathbf{e}\in\mathcal{E}} \left\{ \max_{\mathbf{f}\in\mathcal{F}} \left\{ \min_{\mathbf{a}\in\mathcal{A}(\mathbf{e},\mathbf{f})} \left(\sum_{t=1}^{T} c(\mathbf{a}_t) \right) \right\} \right\}. \tag{2}$$

$\mathbf{f}$ consists of f^t_l and f^t_w. $\mathcal{F}$ is a set and consists of a finite number of $\mathbf{f}$. We have the following theorem.

Theorem 1: problems (1) and (2) have the same optimum, and the optimal solution for problem (1) could be obtained by solving the problem (2).

Proof: The compact forms of problems (1) and (2) without the upper level are presented by (3) and (4), respectively.

$$\max_{p} \ \mathbf{c}^{\mathrm{T}} \cdot \mathbf{p}^* \tag{3a}$$

$$\text{s.t.} \ \sum_{r_t=1}^{R_t} p^t_{r_t,\ r_{t-1}} = 1, \ t \in [T], r_{t-1} \in \left[R_{t-1}\right] \tag{3b}$$

$$0 \le p^t_{r_t,r_{t-1}} \le 1, t \in [T], \ r_{t-1} \in \left[R_{t-1}\right], \ r_t \in [R_t] \tag{3c}$$

$$\max_{v} \ \mathbf{c}^{\mathrm{T}} \cdot \mathbf{v} \tag{4a}$$

$$\text{s.t.} \ 1^{\mathrm{T}} \cdot \mathbf{v} = 1 \tag{4b}$$

$$\mathbf{0} \le \mathbf{v} \le \mathbf{1}. \tag{4c}$$

$\mathbf{c}$, $\mathbf{c} = col(\mathrm{c}_1, \ldots, \mathrm{c}_K) > \mathbf{0}$, is the coefficient vector, and K denotes the number of different combinations of attacks in the middle level. c_i, $i \in [K]$, represent the minimized system cost under different combinations of attacks and are obtained by solving the lower lever problems. $\mathbf{p}^* = col(p^*_1, \ldots, p^*_K)$, where each p^*_i refers to the probability of occurrence of the i-th combinatory of attack, i.e., $p^*_i = \prod_{t=1}^{T} p^t_{r_t,r_{t-1}}$.

Introduce variable $\mathbf{v} = col(v_1, \ldots, v_K)$, and establish one-to-one correspondence between $\mathbf{v}$ and $\mathbf{p}^*$, $\mathbf{v} = \mathbf{p}^*$. Obviously, objective functions (3a) and (4a) are equivalent. By (3b) and the definition of $\mathbf{p}^*$, constraint (4b) holds. We cannot obtain (3b) for all $t \in [T]$, $r_{t-1} \in [R_{t-1}]$ from (4b). Thus, constraint (4b) is the relaxation of (3b). By (3c) and the definition of $\mathbf{p}^*$, constraint (4c) holds. Similarly, we cannot obtain (3c) from (4c). Thus, constraint (4c) is the relaxation of (3c).

Problem (4) is a linear programming (LP) problem. There must exist a *vertex* in its feasible region which is optimal for this problem. Denote one of the maximum elements in vector $\mathbf{c}$ as c_{opt}, i.e., the *opt*-th element in vector $\mathbf{c}$, $opt \in [K]$. By solving (4), we obtain an optimal solution, $col(0, \ldots, 0, 1, 0, \ldots, 0)$, from one of the vertices in its feasible region, where 1 is the value of v_{opt} whose coefficient is c_{opt}.

According to the optimal solution for (4), every $p^t_{r_t,r_{t-1}}$ which v_{opt} consists of equals 1. The rest $p^t_{r_t,r_{t-1}}$ either equal 0 or have no influence on the value of the objective function and can be set to any values satisfying the constraints. Thus, the optimal solution for (3) is obtained from that for (4). Moreover, the upper level of problems (1) and (2) is the same. Thus, Theorem 1 holds. This completes the proof. ■

Compared with the model (1), the tri-level model (2), also known as the two-stage RO model, is easier to be solved. Please refer to the following contents for details.

B. Lower-Level Constraints

Power network constraints in the lower level are:

$$u^t_g \mathrm{P}^{\min}_g \le p^t_g \le u^t_g \mathrm{P}^{\max}_g, g \in \mathcal{G}^p, t \in \mathcal{T} \tag{5}$$

$$u^t_g \mathrm{G}^{\min}_g \le g^t_g \le u^t_g \mathrm{G}^{\max}_g, g \in \mathcal{G}^g, t \in \mathcal{T} \tag{6}$$

$$p^{t+1}_g - p^t_g \le \left(2 - u^t_g - u^{t+1}_g\right)\mathrm{P}^{\max}_g + \left(1 + u^t_g - u^{t+1}_g\right)\mathrm{P}^{\mathrm{u}}_g \tag{7}$$

$$p^t_g - p^{t+1}_g \le \left(2 - u^t_g - u^{t+1}_g\right)\mathrm{P}^{\max}_g + \left(1 - u^t_g + u^{t+1}_g\right)\mathrm{P}^{\mathrm{d}}_g \tag{8}$$

$$g^{t+1}_g - g^t_g \le \left(2 - u^t_g - u^{t+1}_g\right)G^{\max}_g + \left(1 + u^t_g - u^{t+1}_g\right)G^{\mathrm{u}}_g \tag{9}$$

$$g^t_g - g^{t+1}_g \le \left(2 - u^t_g - u^{t+1}_g\right)G^{\max}_g + \left(1 - u^t_g + u^{t+1}_g\right)G^{\mathrm{d}}_g \tag{10}$$

$$u^{t+1}_g \le u^t_g, g \in \mathcal{G}^p \bigcup \mathcal{G}^g, t \in \mathcal{T}\backslash\{T\} \tag{11}$$

$$\left|\theta^t_i\right| \le \theta^{\max}_i, i \in \mathcal{N}^p, t \in \mathcal{T} \tag{12}$$

$$\left|p^t_l\right| \le \mathrm{P}_l, l \in \mathcal{L}^p, t \in \mathcal{T} \tag{13}$$

$$0 \le p^t_d \le \mathrm{P}_d, d \in \mathcal{D}^p, t \in \mathcal{T} \tag{14}$$

$$\mathrm{x}_l p^t_l = \left(1 - f^t_l + e_l f^t_l\right)\left(\theta^t_{i(l)} - \theta^t_{j(l)}\right), l \in \mathcal{L}^p, t \in \mathcal{T} \tag{15}$$

$$\sum_{g_{\mathrm{p}}\in\mathcal{G}^p} p^t_{g_{\mathrm{p}}(i)} + \sum_{g_{\mathrm{g}}\in\mathcal{G}^g} g^t_{g_{\mathrm{g}}(i)} + \sum_{l_1\in\mathcal{L}^p} p^t_{l_1(i)} - \sum_{l_2\in\mathcal{L}^p} p^t_{l_2(i)} = \sum_{d\in\mathcal{D}^p} \mathrm{P}_{d(i)} - \sum_{d\in\mathcal{D}^p} p^t_{d(i)}, i \in \mathcal{N}^p, t \in \mathcal{T}. \tag{16}$$

Constraints (5) and (6) represent the output capacities of traditional and gas-fired units, respectively, and constraints (7)-(10) restrict their ramping capabilities for any $g \in \mathcal{G}^p$ /$\mathcal{G}^g$ and $t \in \mathcal{T}\backslash\{T\}$. Constraint (11) declares that all units cannot be re-started up afterward if they are shut down at time t, due to the limited response time during the hurricane. Constraints (12)-(14) state the boundaries of the phase angle, thermal limit of the power transmission line, and the maximum value of power load shedding, respectively. Equation (15) is the DC power flow constraint with preventive measures e_l and attacks f^t_l at time t, where $i(l)$ and $j(l)$ denote the power transmission line l connecting to nodes i and j, respectively. Equation (16) is the nodal power balance constraint, where $g_p(i)$, $g_g(i)$, $l_1(i)$, $l_2(i)$, and $d(i)$ represent traditional and gas-fired units, the inflow and outflow of a power transmission line, and the load connecting to node i, respectively.

Gas network constraints in the lower level are:

$$0 \le g_w^t \le \left(1 - f_w^t + e_w f_w^t\right) \mathrm{G}_w^{\max}, w \in \mathcal{W}, t \in \mathcal{T} \tag{17}$$

$$0 \le g_{\mathrm{in},s}^t \le \mathrm{G}_s^{\mathrm{in}}, s \in \mathcal{S}, t \in \mathcal{T} \tag{18}$$

$$0 \le g_{\mathrm{out},s}^t \le \mathrm{G}_s^{out}, s \in \mathcal{S}, t \in \mathcal{T} \tag{19}$$

$$0 \le g_s^{t+1} = g_s^t + g_{\mathrm{in},s}^t - g_{\mathrm{out},s}^t \le \mathrm{G}_s^{\max}, s \in \mathcal{S}, t \in \mathcal{T} \backslash \{T\} \tag{20}$$

$$G_i^{\min} \le \pi_i^t \le \mathrm{G}_i^{\max}, i \in \mathcal{N}^g, t \in \mathcal{T} \tag{21}$$

$$0 \le g_d^t \le \mathrm{G}_d, d \in \mathcal{D}^g, t \in \mathcal{T} \tag{22}$$

$$\pi_{j(c)}^t \le \alpha_c \pi_{i(c)}^t, c \in \mathcal{C}^g, t \in \mathcal{T} \tag{23}$$

$$0 \le g_c^t \le \mathrm{G}_c, c \in \mathcal{C}^g, t \in \mathcal{T} \tag{24}$$

$$\left(g_l^t\right)^2 \cdot \mathrm{sgn}\left(\pi_{i(l)}^t, \pi_{j(l)}^t\right) = \mathrm{W}_l \left(\pi_{i(l)}^t - \pi_{j(l)}^t\right) \tag{25a}$$

$$\mathrm{sgn}\left(\pi_{i(l)}^t, \pi_{j(l)}^t\right) = \begin{cases} 1 & \pi_{i(l)}^t \ge \pi_{j(l)}^t \\ -1 & \pi_{i(l)}^t < \pi_{j(l)}^t \end{cases}, \ l \in \mathcal{L}^g, t \in \mathcal{T} \tag{25b}$$

$$\sum_{w \in \mathcal{W}} g_{w(i)}^t + \sum_{l_1 \in \mathcal{L}^g} g_{l_1(i)}^t - \sum_{l_2 \in \mathcal{L}^g} g_{l_2(i)}^t + \sum_{c_1 \in \mathcal{C}^g} g_{c_1(i)}^t - \sum_{c_2 \in \mathcal{C}^g} g_{c_2(i)}^t = \sum_{d \in \mathcal{D}^g} \mathrm{G}_{d(i)} - \sum_{d \in \mathcal{D}^g} g_{d(i)}^t + \sum_{s \in \mathcal{S}} g_{in,s(i)}^t - \sum_{s \in \mathcal{S}} g_{out,s(i)}^t + \sum_{g_g \in \mathcal{G}^g} \gamma_g \cdot g_{g_{\mathrm{g}}(i)}^t, i \in \mathcal{N}^g, t \in \mathcal{T}. \tag{26}$$

Constraint (17) restricts the output capacity of the gas well with preventive measures e_l and attacks f_l^t. Constraints (18)-(20) state the maximum input rate, maximum output rate, and the capacity of the gas storage facility, respectively. Constraint (20) also declares the amount of gas remained in the storage facility. Constraints (21) and (22) denote the ranges of the nodal pressure square and the gas load shedding, respectively. The relation between nodal pressure squares of a compressor, i.e., a gas active pipeline, is denoted by a simplified model (23) [4]–[6], [8], [9], [17], [18], where $j(c)$ and $i(c)$ are its inflow and outflow nodes, respectively. The gas flow in the compressor is restricted by (24). Equation (25), called Weymouth equation, is utilized to depict the relationship between the gas flow and nodal pressure squares in a gas passive pipeline. Derived from the transient-state momentum equation [34], the steady-state Weymouth equation has been widely employed to model the long-distance high-pressure gas passive pipeline [4]–[6], [8]–[10], [17]–[19]. Equation (26) is the nodal gas balance constraint, where $w(i)$, $l_1(i)$, $l_2(i)$, $c_1(i)$, $c_2(i)$, $d(i)$, $s(i)$, and $g_g(i)$ denote gas well, inflow and outflow of gas passive pipeline, inflow and outflow of compressor, gas load, gas storage facility, and gas-fired unit connecting to node i, respectively. $\gamma_g, g \in \mathrm{G}^g$, is the gas-electricity conversion ratio and converts the output of the gas-fired generator into its gas consumption. In the gas network, the gas-fired generator is regarded as the gas load and is the only kind of coupling components interconnecting power and gas networks. This coupling relation is reflected by the last term in (26).

The nonconvexity in equation (25) makes the proposed model computationally intractable. Several piecewise linear methods are employed and compared to address this problem [34]. Test results reveal that the incremental piecewise linear method outperforms the others with promising accuracy and is adopted in this paper. For any $l \in \mathcal{L}_p$ and $t \in \mathcal{T}$, equation (25) is replaced by equation (27).

$$\phi\left(g_l^t\right) \approx \phi\left(\Delta_{l,1}^t\right) + \sum_{m \in [M]} \left(\phi\left(\Delta_{l,m+1}^t\right) - \phi\left(\Delta_{l,m}^t\right)\right) \sigma_{l,m}^t \tag{27a}$$

$$g_l^t = \Delta_{l,1}^t + \sum_{m \in [M]} \left(\Delta_{l,m+1}^t - \Delta_{l,m}^t\right) \sigma_{l,m}^t \tag{27b}$$

$$\sigma_{l,m+1}^t \le \delta_{l,k}^t \le \sigma_{l,m}^t, m \in [M-1] \tag{27c}$$

$$0 \le \sigma_{l,m}^t \le 1, m \in [M], \tag{27d}$$

where $\Delta_{l,m}^t$ are piecewise segments and are constants. $\sigma_{l,m}^t$ and $\delta_{l,m}^t$ are auxiliary continuous and binary variables, respectively. $\phi(\cdot)$ is a function which maps the $g_l^t/\Delta_{l,m}^t$ into the nonlinear term of (25a). We have $\mathcal{A} := \{\mathbf{a} |$ (25)-(24) and (26)-(27)$\}$.

C. Middle-Level Constraints

In the middle level, the uncertainty set is constructed by combining the data-based method (see Section II-B) with the Markov property of the hurricane (see Section II-A). Firstly, according to the historical or forecast data, the direction, range, and intensity of a hurricane are estimated, and the region partition of an IEGS is obtained. Then, according to the above information, the Markov property of a hurricane is utilized to construct the data-based uncertainty set, in which the following rules are respected: i) there is one and only one region being attacked at each time t; ii) if the attacked region includes more than one component, all of them are regarded as a whole and will be attacked simultaneously; iii) only neighboring regions and the same regions may be attacked sequentially. In the data-based uncertainty set, the rules i)-iii) are denoted by (28)-(30), respectively.

$$\sum_{i \in \mathcal{U}^t} h_i^t\left(\mathcal{F}_i^t\right) = 1 t \in \mathcal{T} \tag{28}$$

$$\mathcal{F}_i^t = \begin{cases} (0, \ldots, 0)^{\mathrm{T}} \ h_i^t\left(\mathcal{F}_i^t\right) = 0 \\ (1, \ldots, 1)^{\mathrm{T}} \ h_i^t\left(\mathcal{F}_i^t\right) = 1 \end{cases} \ i \in \mathcal{U}^t, t \in \mathcal{T} \tag{29}$$

$$h_{i'}^{t+1}\left(\mathcal{F}_{i'}^{t+1}\right) \le 1 - h_i^t\left(\mathcal{F}_i^t\right), t \in \mathcal{T} \backslash \{T\}, i \in \mathcal{U}^t, i' \notin \mathcal{U}_{i,Nei.}^{t+1}. \tag{30}$$

$\mathcal{F}_i^t$ is a set consisting of the binary variables f_l^t and f_w^t whose corresponding power transmission line l and the gas well w belong to region i at t. n_i^t is the total number of elements in $\mathcal{F}_i^t$. $h_i^t(\cdot)$ maps the n_i^t-dimension domain $\{(0, \ldots, 0)^{\mathrm{T}}, (1, \ldots, 1)^{\mathrm{T}}\}$ to the one-dimension set $\{0, 1\}$. $\mathcal{U}_{i,Nei.}^{t+1}$ consists of all neighboring regions and the same region of region i at $t+1$. Although having a complex form, in fact, constraints (28)-(30) are affine functions of f_l^t and f_w^t. In addition, f_l^t and f_w^t need to satisfy

$$f_l^\tau = 0, \tau \in [t-1], \{l, t\} \in \mathcal{H}_{\mathrm{L}} \tag{31a}$$

$$f_l^\tau = f_l^t, \tau \in \mathcal{T} \backslash [t], \{l, t\} \in \mathcal{H}_{\mathrm{L}} \tag{31b}$$

$$f_w^\tau = 0, \tau \in [t-1], \{w, t\} \in \mathcal{H}_{\mathrm{W}} \tag{31c}$$

$$f_w^\tau = f_w^t, \tau \in \mathcal{T} \backslash [t], \{w, t\} \in \mathcal{H}_{\mathrm{W}}. \tag{31d}$$

$\mathcal{H}_{\mathrm{L}}$ and $\mathcal{H}_{\mathrm{W}}$ are the sets consisting of elements $\{l, t\}$ $(l \in \mathcal{L}^p)$ and $\{w, t\}$ $(w \in \mathcal{W})$, respectively. Sets $\{l, t\}$ and $\{w, t\}$ denote the power transmission line l and the gas well w whose regions

are at time t, respectively. For example, in Fig. 1, Line 3 can be denoted as $\{l_3, 2\}$. Overall, the data-based uncertainty set is denoted by $\mathcal{F} \coloneqq \{\mathbf{f}|\ (28)-(31)\}$.

Different from [35], the proposed uncertainty set $\mathcal{F}$ consists of a finite number of scenarios. The conservativeness of an RO model consisting of a scenario-based uncertainty set could be reduced effectively by removing redundant scenarios. In the proposed uncertainty set, the redundant scenarios are excluded by combining the historical or forecast data with the Markov property of the hurricane, which leads to a less conservative RO model. For example, in Fig. 1, Scenario 1 and Scenario 2 are included in the data-based uncertainty set, while Scenario 3, which could not occur due to the Markov property of the hurricane, is the redundant scenario and thus is excluded from the proposed uncertainty set.

D. Upper-Level Constraints

In the upper level, system planners harden the critical components in advance to prevent them from being destroyed. Considering the limited budgets, only parts of the components are protected. This relationship is denoted by

$$\sum_{l} e_l + \sum_{w} e_w \le \mathrm{E}_{\mathrm{total}}, \tag{32}$$

and we have the defense set $\mathcal{E}$, $\mathcal{E} \coloneqq \{\mathbf{e}|(32)\}$.

E. Model Extension

The proposed model has the potential to accommodate the following scenarios by simple extensions.

1) *Investment Cost:* The investment cost is not considered in the objective function (2). However, from an economic perspective, a balance between the investment cost and the system cost is significant. The proposed model can be extended to achieve this goal by replacing (2) with

$$\phi_T^*(\mathbf{e},\mathbf{f},\mathbf{a}) = \min_{\mathbf{e}\in\mathcal{E}}\left\{\sum_{t=1}^{T}\left(\sum_{l\in\mathcal{L}^p} c_l e_l^t + \sum_{w\in\mathcal{W}} c_w e_w^t\right) + \max_{\mathbf{f}\in\mathcal{F}}\left\{\min_{\mathbf{a}\in\mathcal{A}(\mathbf{e},\mathbf{f})}\left(\sum_{t=1}^{T} c(\mathbf{a}_t)\right)\right\}\right\}, \tag{33}$$

where c_l and c_w are the investment cost of preventive measures for power transmission line l and gas well w, respectively. This extended model is further investigated in Section V-C.

2) *Other Extreme Events:* It is assumed that the hurricane has no influence on power units or gas pipelines. However, they may not survive from some other extreme events, such as earthquakes and deliberate human attacks. The proposed model can be extended to accommodate these extreme events by replacing (11), (24) and (25a) with

$$u_g^{t+1} \le u_g^t,\ g \in \mathcal{G}^p \bigcup \mathcal{G}^g,\ t \in \mathcal{T}\backslash\{T\} \tag{34a}$$

$$u_g^t \le 1 - f_g^t + e_g f_g^t,\ g \in \mathcal{G}^p \bigcup \mathcal{G}^g,\ t \in \mathcal{T} \tag{34b}$$

$$0 \le g_c^t \le \left(1 - f_c^t + e_c f_c^t\right)\mathrm{G}_c,\ c \in \mathcal{C}^g,\ t \in \mathcal{T} \tag{35}$$

$$\left(g_l^t\right)^2 \cdot \mathrm{sgn}\left(\pi_{i(l)}^t, \pi_{j(l)}^t\right) = \mathrm{W}_l\left(1 - f_l^t + e_l f_l^t\right)\left(\pi_{i(l)}^t - \pi_{j(l)}^t\right),\quad l \in \mathcal{L}_g,\ t \in \mathcal{T}, \tag{36}$$

where f_g^t/e_g, f_c^t/e_c, and f_l^t/e_l are binary variables which denote if the power unit, compressor, and gas passive pipeline are attacked at time t/are protected or not, respectively. In addition, f_g^t, f_c^t, f_l^t and e_g, e_c, e_l should be added to the data-based uncertainty set $\mathcal{F}$ and defense set $\mathcal{E}$, respectively. The bilinear terms in (36) can be addressed using the *Big-M* method [18].

3) *Multi-Region Attacks:* It is assumed that the hurricane only strikes one region at each time t ($t \in \mathcal{T}$). Sometimes, multiple regions near each other may suffer from hurricane strikes simultaneously. The proposed model can be extended to incorporate multi-region attacks by replacing (28) and (30) with

$$\sum_{i\in\mathcal{U}^t} h_i^t\left(\mathcal{F}_i^t\right) = \mathrm{F}^t,\ t \in \mathcal{T} \tag{37}$$

$$h_i^t\left(\mathcal{F}_i^t\right) \cdot h_{i'}^t\left(\mathcal{F}_{i'}^t\right) = 0,\ t \in \mathcal{T},\ i \in \mathcal{U}^t,\ i' \notin \tilde{\mathcal{U}}_{i,Nei.}^{t,\mathrm{F}^t} \tag{38a}$$

$$h_{i'}^{t+1}\left(\mathcal{F}_{i'}^{t+1}\right) \le 1 - h_i^t\left(\mathcal{F}_i^t\right),\ t \in \mathcal{T}\backslash\{T\},\ i \in \mathcal{U}_C^t,\ i' \notin \mathcal{U}_{i,Nei.}^{t+1}, \tag{38b}$$

where F^t, a positive integer, is the number of attacked regions at t. $\tilde{\mathcal{U}}_{i,Nei.}^{t,\mathrm{F}^t}$ is a generalization of the set $\mathcal{U}_{i,Nei.}^t$ and consists of the same region i and the nearest $2 \cdot (\mathrm{F}^t - 1)$ neighboring regions (if applicable) of region i at t. For example, for $t = 2$, $\mathrm{F}^t = 2$, and $i = 3$ in Fig. 1, $\tilde{\mathcal{U}}_{i,Nei.}^{t,\mathrm{F}^t} = \{2, 3, 4\}$. $\mathcal{U}_C^t$, $\mathcal{U}_C^t = \{(1/|\mathcal{U}^t|) \cdot (\sum_{i\in\mathcal{U}^t} i \cdot h_i^t(\mathcal{F}_i^t))\}$, consists of only one element, i.e., the region where the center of the hurricane lies.

IV. Solution Method

The compact form of the proposed two-stage RO model (consisting of (2), (5)-(24), and (26)-(32)) is presented by

$$\min_{\mathbf{e}}\ \left\{\max_{\mathbf{f}}\left\{\min_{\mathbf{x},\mathbf{z}} \mathbf{c}^{\mathrm{T}} \cdot \mathbf{x}\right\}\right\} \tag{39a}$$

$$\text{s.t.}\ \ \mathbf{1}^{\mathrm{T}} \cdot \mathbf{e} \le \mathrm{E}_{\mathrm{total}} \tag{39b}$$

$$\mathbf{F} \cdot \mathbf{f} \le \left[\mathbf{1}^{\mathrm{T}}, \mathbf{0}^{\mathrm{T}}\right]^{\mathrm{T}} \tag{39c}$$

$$\mathbf{R}(\mathbf{e},\mathbf{f}) \cdot \mathbf{x} + \mathbf{S} \cdot \mathbf{z} \le \mathbf{h}(\mathbf{e},\mathbf{f}), \tag{39d}$$

where vectors $\mathbf{x}$ and $\mathbf{z}$ consist of continuous and binary variables, respectively. $\mathbf{c}$ is the coefficient vector. $\mathbf{F}$ and $\mathbf{S}$ refer to (constant) coefficient matrices. $\mathbf{R}(\mathbf{e}, \mathbf{f})$ and $\mathbf{h}(\mathbf{e}, \mathbf{f})$ are the coefficient matrix and vector with upper and middle level variables $\mathbf{e}$ and $\mathbf{f}$, respectively. $\mathbf{1}$ and $\mathbf{0}$ are all one and all zero vectors, respectively. Equations (39a)-(39d) are corresponding to compact forms of the objective function (2), the upper-level constraints (32), middle-level constraints (28)-(31), and lower-level constraints (5)-(24) and (26)-(27), respectively.

Some algorithms are used to solve two-stage RO problems, e.g., Benders decomposition [35] and C&CG [16]. However, these algorithms suffer from convergence issues if binary variables exist in the lower level. The nested C&CG algorithm, whose convergence is proved in [36], is adopted in this paper to solve the proposed model. Details are as follows.

Subproblem: Inner C&CG With the Preventive Measures $\mathbf{e}^*$

Step 1 Set $LB_{\text{in}} = \mathbf{c}^{\text{T}} \cdot \mathbf{x}^*$, $UB_{\text{in}} = +\infty$, $K_{\text{in}} = 1$, $\text{z}_1^* = \text{z}^*$, ε_{in}. Find a legal attack scenario $\mathbf{f}^*$, and solve the lower level problem

$$\min_{\mathbf{x},\,\mathbf{z}} \quad \mathbf{c}^{\text{T}} \cdot \mathbf{x} \tag{40a}$$

$$\text{s.t.} \quad \mathbf{R}(\mathbf{e}^*, \mathbf{f}^*) \cdot \mathbf{x} \le \mathbf{h}(\mathbf{e}^*, \mathbf{f}^*) - \mathbf{S} \cdot \mathbf{z}. \tag{40b}$$

Obtain the solution ($\mathbf{x}^*$, $\mathbf{z}^*$). Set $LB_{\text{in}} = \mathbf{c}^{\text{T}} \cdot \mathbf{x}^*$, $\text{z}_1^* = \text{z}^*$, $\text{f}_{\text{opt}}^* = \text{f}^*$.
Step 2 Solve the middle level problem with dual variable $\boldsymbol{\lambda}_k$

$$\max_{\vartheta,\mathbf{f},\boldsymbol{\lambda}_k} \quad \vartheta \tag{41a}$$

$$\text{s.t.} \quad \vartheta \le (\mathbf{h}(\mathbf{e}^*, \mathbf{f}) - \mathbf{S} \cdot \mathbf{z}_k^*)^{\text{T}} \cdot \boldsymbol{\lambda}_k, k \in [K_{\text{in}}] \tag{41b}$$

$$\mathbf{R}(\mathbf{e}^*, \mathbf{f})^{\text{T}} \cdot \boldsymbol{\lambda}_k \le \mathbf{c}, k \in [K_{\text{in}}] \tag{41c}$$

$$\boldsymbol{\lambda}_k \le \mathbf{0}, k \in [K_{\text{in}}], \mathbf{F} \cdot \mathbf{f} \le \mathbf{1}. \tag{41d}$$

Obtain the updated $\mathbf{f}^*$ and the optimum ϑ^*. Set $UB_{\text{in}} = \vartheta^*$.
Step 3 Solve the problem (40) with updated $\mathbf{f}^*$. Obtain the solution ($\mathbf{x}^*$, $\mathbf{z}^*$). If $LB_{\text{in}} \le \mathbf{c}^{\text{T}} \cdot \mathbf{x}^*$, set $\mathbf{f}_{\text{opt}}^* = \mathbf{f}^*$. Otherwise, $\mathbf{f}_{\text{opt}}^*$ remains unchanged. Set $LB_{\text{in}} = \max(LB_{\text{in}}, \mathbf{c}^{\text{T}} \cdot \mathbf{x}^*)$.
Step 4 Check if $UB_{\text{in}} - LB_{\text{in}} \le \varepsilon_{\text{in}}$. If yes, set $\text{Opt}_{\text{in}} = \vartheta^*$ and return $\mathbf{f}_{\text{opt}}^* = \mathbf{f}^*$ and Opt_{in} to the Master Problem. Otherwise, set $\text{z}_{K_{\text{in}}}^* = \text{z}^*$, $K_{\text{in}} = K_{\text{in}} + 1$, and add new constraints with dual variable $\boldsymbol{\lambda}_{\text{K}_{\text{in}}}$

$$\vartheta \le (\mathbf{h}(\mathbf{e}^*, \mathbf{f}) - \mathbf{S} \cdot \mathbf{z}_{K_{\text{in}}}^*)^{\text{T}} \cdot \boldsymbol{\lambda}_{K_{\text{in}}} \tag{42a}$$

$$\mathbf{R}(\mathbf{e}^*, \mathbf{f})^{\text{T}} \cdot \boldsymbol{\lambda}_{K_{\text{in}}} \le \mathbf{c}, \boldsymbol{\lambda}_{K_{\text{in}}} \le \mathbf{0} \tag{42b}$$

to (41). Then, go to Step 2.

The procedures to solve Master Problem (MP) are as follows.

Master Problem: Outer C&CG With the Potential Attacks $\mathbf{f}^*$

Step 1 Find legal preventive measures $\mathbf{e}^*$. Solve Subproblem. Obtain $\mathbf{f}_{\text{opt}}^*$ and Opt_{in}. Set $LB_{\text{out}} = -\infty$, $UB_{\text{out}} = \text{Opt}_{\text{in}}$, $\mathbf{f}_1^* = \mathbf{f}_{\text{opt}}^*$, $K_{\text{out}} = 1$, $\mathbf{e}_{\text{opt}}^* = \mathbf{e}^*$, ε_{out}.
Step 2 Solve the upper level problem:

$$\min_{\zeta,\mathbf{e},\mathbf{x}_k,\mathbf{z}_k} \quad \zeta \tag{43a}$$

$$\text{s.t.} \quad \zeta \ge \mathbf{c}^{\text{T}} \cdot \mathbf{x}_k, k \in [K_{\text{out}}] \tag{43b}$$

$$\mathbf{R}(\mathbf{e}, \mathbf{f}_k^*) \cdot \mathbf{x}_k + \mathbf{S} \cdot \mathbf{z}_k \le \mathbf{h}(\mathbf{e}, \mathbf{f}_k^*), k \in [K_{\text{out}}] \tag{43c}$$

$$\mathbf{1}^{\text{T}}\mathbf{e} \le \text{E}_{\text{total}}. \tag{43d}$$

Obtain the updated $\mathbf{e}^*$ and optimum ζ^*. Set $LB_{\text{out}} = \zeta^*$, $\mathbf{e}_{\text{opt}}^* = \mathbf{e}^*$. Stop if $UB_{\text{out}} - LB_{\text{out}} = \varepsilon_{\text{out}}$. Otherwise, go to Step 3.
Step 3 Solve Subproblem with updated $\mathbf{e}^*$. Obtain $\mathbf{f}_{\text{opt}}^*$ and Opt_{in}. Set $UB_{\text{out}} = \min(UB_{\text{out}}, \text{Opt}_{\text{in}})$.
Step 4 Check if $UB_{\text{out}} - LB_{\text{out}} \le \varepsilon_{\text{out}}$. If yes, stop and obtain preventive measures and re-dispatch decisions. Otherwise, set $K_{\text{out}} = K_{\text{out}} + 1$ and $\mathbf{f}_{\text{K}_{\text{out}}}^* = \mathbf{f}^*$, and add new constraints with new variables $\mathbf{x}_{\text{K}_{\text{out}}}$ and $\mathbf{z}_{\text{K}_{\text{out}}}$

$$\zeta \ge \mathbf{c}^{\text{T}} \cdot \mathbf{x}_{K_{\text{out}}} \tag{44a}$$

$$\mathbf{R}(\mathbf{e}, \mathbf{f}_k^*) \cdot \mathbf{x}_{K_{\text{out}}} + \mathbf{S} \cdot \mathbf{z}_{K_{\text{out}}} \le \mathbf{h}(\mathbf{e}, \mathbf{f}_k^*) \tag{44b}$$

to (43). Then, go to Step 2.

The above Sub-Master framework is implemented iteratively. Bilinear terms in (41b), (41c), and (43c) are linearized using the *Big-M* method [18]. After the linearization, models (40), (41), and (43) become mixed-integer linear programming (MILP) problems and can be effectively solved by some commercial solvers, such as Gurobi. Moreover, the convergence of the nested C&CG algorithm is also guaranteed. Note that the nested C&CG algorithm is valid, providing the lower level problem is always feasible for any $\mathbf{e} \in \mathcal{E}$ and $\mathbf{f} \in \mathcal{F}$ [36].

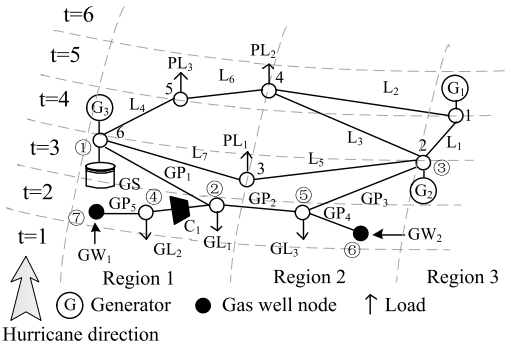

Fig. 3. 6-bus power network and 7-node gas network with the region partition.

Note that the values of *Big-M* are vital for the algorithmic efficiency. Large value enlarges the search space and increases the computational cost. Small value shrinks the primal feasible region, and the optimal solution may be missing. The values of *Big-M* in (43c) are apparent since the ranges are determined by the constraints introduced in Section III-B. However, choosing *Big-M* values for (41b) and (41c) is tricky, as we do not know the lower bounds of the dual variables. In this paper, a novel method proposed in [18] is adopted to decide *Big-M* values. The idea is that scaling the objective function by a positive number does not influence the optimal solution. Besides, the boundaries of the variables generated by the *Big-M* method are relevant to the optimum. Thus, their boundaries are reduced effectively if the objective function is divided by a large positive number.

V. Case Studies

The proposed model is tested on two systems, one with a 6-bus power network and a 7-node gas network, and the other with a 39-bus power network and a 20-node gas network. Both simulations are coded in MATLAB R2017a and performed on a PC with an i5-6500 CPU at 3.2 GHz and 16 GB memory. Gurobi 7.5.1 is chosen as the solver.

A. 6-Bus Power Network and 7-Node Gas Network

Preventive hardening is implemented in the 6-bus power network and a 7-node gas network. Historical hurricane data on Louisiana (listed in Section II-B) are used to obtain the region partition on this IEGS, which is presented in Fig. 3. PL, GL, L, GP, and C denote power loads, gas loads, power transmission lines, gas passive pipelines, and compressors, respectively. G_2 and G_3 are gas-fired units, and G_1 is the traditional unit. Assuming attacks occur at six discrete times, i.e., $T = 6$, and the interval between two consecutive attacks is 20 minutes. The number of segments M is set to 8. Convergence thresholds, ε_{in} and ε_{out}, are both 0.1%. Detailed data of this integrated system are in [18]. Different load levels are shown in Table III.

TABLE III
LOAD LEVELS OF 6-BUS POWER NETWORK AND 7-NODE GAS NETWORK

Load		Load level (power, gas)	Abbreviation
Power (MW)	Gas (Sm^3/h)		
283	6920	middle, high	M-H
256	5360	middle, middle	M-M
336	6680	high, high	H-H
201	4180	low, low	L-L

TABLE IV
INFLUENCE OF DIFFERENT DEFENSE BUDGETS

No. of D	System cost ($*10^4$ \$)	Cost (%)	Attacked region				Power load shed (MW·h)	Gas load shed ($*10^3$ Sm^3)
			t=2	t=3	t=4	t=5		
0	13.67	100	R1	R1	R2	R2	137.3	0.45
1	11.14	80.94	R1	R2	R1	R1	126.0	1.49
2	4.11	28.04	R1	R1	R1	R2	36.0	1.49
3	1.72	10.04	R2	R2	R3	R2	0	3.37
4	0.51	0.89	R2	R2	R1	R1	1.2	0
≥ 5	0.39	0	R2	R2	R2	R1	0	0

B. Influence of Defense Budgets

The influence of defense budgets is shown in Table IV. The load level is set to M-M. No. of D denotes the number of defense budgets. Cost (%) is calculated by

$$\text{cost}(\%) = \frac{\text{corresponding cost} - \text{operation cost}}{(\text{cost of D} = 0) - \text{operation cost}} \cdot 100\%, \tag{45}$$

where the "corresponding cost" is the optimal system cost under a fixed No. of D, i.e., the optimum of the proposed model under a fixed No. of D. "Operation cost" is the optimal system cost without the influence of any events, i.e., the optimal cost when all components in the IEGS can work normally. "Cost of D = 0" is the optimal system cost when No. of D = 0, i.e., the optimum of the proposed model when No. of D = 0. Region 1 and Region 2 in Fig. 3 are short for R1 and R2, respectively.

As is shown in the table, the system cost drops dramatically when No. of D increases at first, followed by a gentle decrease trend. The cost caused by both *power and gas load shedding* becomes zero (Cost (%) = 0) when No. of D $\geq$ 5. Namely, the hurricane does not cause loss of load, though some components are not protected. This phenomenon reveals that there do exist critical components in a system. In fact, the system cost is not equal to zero when No. of D $\geq$ 5, due to the cost arising from power generators and gas wells.

C. Influence of the Investment Cost

The proposed model (without the investment cost) and the extended model introduced in Section III-E 1) (with the investment cost) are compared. Fig. 4 shows the test results. The semi-logarithmic coordinate system is adopted to capture the slight decline of the system cost when No. of D becomes larger. As is shown in Fig. 4 (a), the decreasing trend in the system cost is similar under all load levels when No. of D increases. However, a reasonable No. of D (referred to as the *inflection point*), i.e., a balance between the investment cost and system cost, cannot be easily observed. Differently, the inflection point is shown clearly in Fig. 4 (b), i.e., No. of D = 2 for L-L and No. of D=4 for the other load levels.

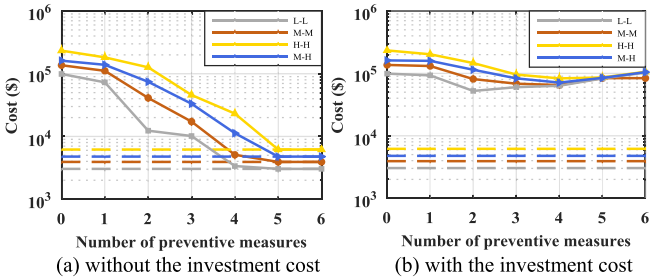

(a) without the investment cost (b) with the investment cost

Fig. 4. Influence of defense budgets under different load levels.

TABLE V
PROTECTED COMPONENTS

No. of D \ Load level	M-H	M-M	H-H	L-L
1	L_2	L_2	L_2	L_3
2	L_2, L_6	L_3, L_6	GW_1, L_2	L_2, L_6
3	GW_1, L_2, L_6	L_2, L_4, L_6	GW_1, L_2, L_6	GW_2, L_2, L_6
4	GW_1, GW_2, L_3, L_6	GW_1, GW_2, L_2, L_6	GW_1, GW_2, L_3, L_6	GW_1, GW_2, L_2, L_6
5	GW_1, GW_2, L_2, L_4, L_6	GW_1, GW_2, L_2, L_4, L_6	GW_1, GW_2, L_2, L_4, L_6	GW_1, GW_2, L_2, L_4, L_6

As a complement to Fig. 4 (a), specific preventive measures are listed in Table V. Though sharing a similar *decreasing trend* under different load levels regarding the system cost, preventive measures are quite different when No. of D is smaller than 5. This result indicates that the critical components in the IEGS are not fixed and are closely related to load levels. Interestingly, the preventive measures, GW_1, L_2, and L_6, in Fig. 4 (b) when load level is M-M and No. of D = 3 are different from those in Fig. 4 (a) and result in more load shedding, as hardening GW_1, L_2, and L_6 leads to the lowest *total cost* than hardening L_2, L_4, and L_6. However, due to the influence of the investment cost, it fails to find out the most critical components in the IEGS for the hurricane strike scenario.

Compared with the extended model in Section III-E 1), the proposed model (with the objective (2)): i) provides a flexible schema for system planners to decide No. of D when facing the destructive hurricane; ii) always provides optimal preventive measures against the sequential and regional hurricane strike. In the following cases, the proposed model (with the objective (2)) is adopted.

D. Comparison With Other Models

The proposed defense-attack-defense (DAD) model is compared with the other two models. One is the attack-defense (AD) model [37]. Compared with the proposed tri-level DAD model, the bi-level AD model, which has a max-min structure, does not include the upper level and cannot provide optimal preventive measures for the IEGS. In order to make these two models comparable, i) the uncertainty set $\mathcal{F}$ is still adopted in the AD model, i.e., the attacked components which lead to the largest system cost can be obtained; ii) the

TABLE VI
COMPARISON BETWEEN DAD MODEL AND AD MODEL

Load level	System cost (*10^4 $)		Protected components		Load shed (MW·h, *10^3 Sm^3)	
	DAD	AD	DAD	AD	DAD	AD
M-H	1.13	9.83	GW_1, GW_2, L_3, L_6	GW_2, L_2, L_3, L_7	6.6, 0	82.7, 7.24
M-M	0.51	7.71	GW_1, GW_2, L_2, L_6	GW_2, L_2, L_3, L_7	1.2, 0	69.5, 4.63
H-H	2.31	12.66	GW_1, GW_2, L_3, L_6	GW_2, L_2, L_3, L_7	17.2, 0	112.0, 7.63
L-L	0.34	6.71	GW_1, GW_2, L_2, L_6	GW_1, L_2, L_3, L_5	0, 0	72.3, 1.16

TABLE VII
COMPARISON BETWEEN DAD MODEL AND DAD* MODEL

Load level	System cost (*10^5 $)		Attacked components		Load shed (MW·h, *10^3 Sm^3)	
	DAD	DAD*	DAD	DAD*	DAD	DAD*
M-H	1.39	2.02	GW_1, L_4, L_5, L_6	GW_1, GW_2, L_5, L_6	153.0, 2.70	191.9, 11.53
M-M	1.11	1.81	GW_1, L_4, L_5, L_6	L_4, L_5, L_6, L_7	126.0, 1.49	204.8, 0
H-H	1.83	2.48	GW_1, L_4, L_5, L_6	GW_1, GW_2, L_5, L_6	206.0, 2.30	246.5, 11.13
L-L	0.73	1.41	GW_1, L_4, L_5, L_6	L_4, L_5, L_6, L_7	80.7, 1.16	160.8, 0

attacked components (four components according to Fig. 3) in the AD model are protected; iii) No. of D is set to 4 in the DAD model (defensive budgets in both models being identical). Denote C_{DAD} and C_{AD} as the system cost of DAD and AD models, respectively, and corresponding preventive measures are denoted by D_{DAD} and D_{AD}. Theoretically, D_{DAD} is globally optimal, while D_{AD} is a feasible solution. Thus, $C_{DAD} \leq C_{AD}$ always holds. Simulation results are shown in Table VI. C_{AD} far exceeds C_{DAD} under all load levels (at least 4.47 times larger). According to the protected components in the DAD model, GW_1 and GW_2 are critical when No. of D = 4. According to the region partition in Fig. 3, the hurricane could strike at most one gas well. Thus, in the AD model, the other gas well is not protected. This test fully demonstrates the advantage of the proposed model, which can obtain optimal preventive measures.

In addition, the importance of the Markov property is revealed by comparing the DAD model with DAD* model, in which neither the sequential property nor the regional property is respected. Denote C_{DAD} and C_{DAD*} as the system cost of DAD and DAD* models, respectively. It is trivial that $C_{DAD} \leq C_{DAD*}$. Table VII shows the comparison results. No. of D is set to 1. In the DAD* model, the hurricane can strike arbitrary gas wells at $t = 2$ and power transmission lines at $t = 3$ within a limited number of attack budgets. We observe that C_{DAD*} is at least 1.36 times as large as C_{DAD}. Reasons may arise from: i) sequential property: the outage period of some power transmission lines is longer than the actual situation, e.g., L_6 should be destroyed at $t = 5$ rather than $t = 3$; and ii) regional property: there exists more than one region being attacked at the same time, such as GW_1 and GW_2. Actually, this scenario never occurs since these two gas wells are far away from each other. According to the preceding analysis, the conservativeness of the proposed model is greatly reduced by adopting the data-based uncertainty set.

E. 39-Bus Power Network and 20-Node Gas Network

Emergency hardening is implemented in the 39-bus power network and a 20-node gas network. Actual data of hurricane Katrina from its landfall (at Louisiana) to Meridian, Mississippi, are utilized as forecast data and listed in Table VIII. According to the emergency hardening method, the region partition of this IEGS is obtained (presented in Fig. 5). GS and C represent gas storage facility and compressor, respectively. G31, G32, and G39 are gas-fired units, and others denote traditional units. T is set to 9. The attack interval remains 20 minutes. The number of segments M is set to 4. According to [18], the convergence thresholds, ε_{in} and ε_{out}, are set to 0.9% to balance the accuracy and computational burden. Load levels are divided into H-M (1500 MW-1200 Sm^3/h), M-M (1200 MW-1100 Sm^3/h), H-H (1600 MW-1500 Sm^3/h), and L-L (900 MW-950 Sm^3/h).

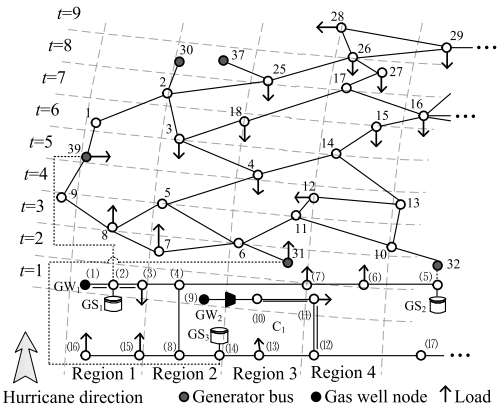

Fig. 5. 39-bus power network and 20-node gas network with region partition.

TABLE VIII
DATA OF HURRICANE KATRINA

Name	Landfall	Category	Duration as Category 3	Direction	Intensity	Forecast horizon
Katrina	Louisiana	3	240 km	S	190 km/h	48 h

F. Influence of Defense Budgets

We continue to investigate the influence of defense budgets. Test results are shown in Fig. 6. The rectangular coordinate system is adopted to capture the overall declining trend. Solid lines on the left part of the figure are the actual system cost, while dotted lines on the right are the estimated value. Dashed lines denote the optimal system cost under normal state. Similar to the results in Section V-B of this section, the system cost drops at an approximately exponential rate under all load levels. Costs (%) are from 7.76 to 14.15 when No. of D = 5, which is acceptable facing such a devastating hurricane. This result indicates that we do not need to protect all

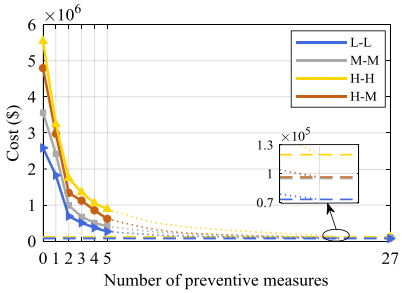

Fig. 6. Influence of defense budgets under different load levels.

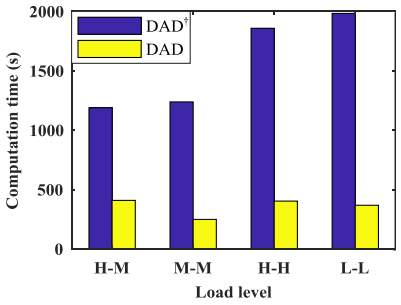

Fig. 7. Computation time of DAD and DAD† models.

TABLE IX
PROTECTED COMPONENTS AND ATTACKED REGION

Load level	Protected components	Attacked region								
		t=1	t=2	t=3	t=4	t=5	t=6	t=7	t=8	t=9
H-M	GW_1, $L_{5\text{-}8}$, $L_{25\text{-}26}$	R2	R1	R2	R3	R4	R4	R4	R4	R4
M-M	GW_1, GW_2, $L_{5\text{-}8}$	R2	R3	R3	R3	R4	R4	R4	R4	R4
H-H	GW_1, $L_{5\text{-}8}$, $L_{25\text{-}26}$	R2	R1	R2	R3	R4	R4	R4	R4	R4
L-L	GW_1, GW_2, $L_{5\text{-}8}$	R2	R3	R3	R3	R4	R4	R4	R4	R4

TABLE X
COMPARISON BETWEEN DAD MODEL AND DAD† MODEL

Load level	System cost (*10^6 $)		Load shed (MW·h, *10^3 Sm^3)	
	DAD	DAD†	DAD	DAD†
M-H	1.34	2.03	224.0, 105.53	357.5, 1.09
M-M	0.99	1.59	143.0, 1.17	274.2, 1.00
H-H	1.74	2.35	288.7, 160.47	393.9, 1.78
L-L	0.69	1.29	91.7, 0.99	223.0, 0.86

components in the IEGS, as there is no load shedding when No. of D $\geq m$ ($m < 27$).

As a complement to Fig. 6, we list parts of the protected components and attacked regions under different load levels in Table IX. No. of D is 3. L_{a-b} denotes the power transmission line connecting power nodes a and b (see Fig. 5). Region 1 to region 4 in Fig. 5 are denoted by R1 to R4, respectively. Intuitively, gas wells are the most critical components in the IEGS, since the attacking towards gas wells reduces the total amount of dispatchable natural gas. However, according to test results, hardening L_{25-26} receives higher returns than protecting GW_2 under the proposed robust framework when both loads reach relatively high levels (H-M and H-H).

G. Comparison With the DAD† Model

In the DAD† model, the regional property of the hurricane is no longer respected. For example, the impossible scenario in Fig. 1 becomes possible. Different from the DAD* model, the sequential property is still considered in the DAD† model. Denote C_{DAD} and $C_{DAD^\dagger}$ as the system cost of DAD and DAD† models, respectively. The relation $C_{DAD} \leq C_{DAD^\dagger}$ always holds. Experimental results are shown in Table X. No. of D is set to 2. Compared with C_{DAD}, $C_{DAD^\dagger}$ increases significantly for all load levels (1.59 times on average). Specifically, power transmission lines 2-3 in Region 1 and 26-27 in Region 4 are attacked at $t = 6$ and 7, respectively, which could never occur considering the reasonable region partition. This verifies the effectiveness of the data-based uncertainty set in reducing the conservativeness of the RO model.

In addition, the proposed DAD model also outperforms the DAD† model in terms of computation time. Denote T_{DAD} and $T_{DAD^\dagger}$ as the computation time of DAD and DAD† models, respectively. Theoretically, the search space of the DAD model in the middle level is smaller than that of the DAD† model, and the search spaces of both models in the upper level keep the same. So, $T_{DAD} < T_{DAD^\dagger}$. Comparison results are shown in Fig. 7. No. of D is set to 2. It is clear that the size of the search space has a huge impact on computation time.

TABLE XI
COMPUTATION TIME (S)

Load \ No. of D	0	1	2	3	4	5
H-M	373	326	409	557	1728	2427
M-M	301	360	249	769	970	1036
H-H	203	224	403	673	1923	2522
L-L	326	468	368	645	807	1150

H. Computation Time and Approximate Solution

The computation times under different load levels and No. of D are compared and listed in Table XI. The computational cost becomes huge when defense budgets are large, as the number of combinations of protected components increases sharply when No. of D rises. This increase is inevitable since the MILP problem is NP-hard. However, the acceptable computation time can still be obtained by leveraging its unique property, e.g., the Markov property, to reduce scenarios in the uncertainty set.

In order to further reduce the computation burden for a large No. of D, a plausible idea is to shrink search spaces in both upper and middle levels to obtain a high-quality approximate solution, and this shrinking strategy is implemented in the DAD‡ model. Table XII shows the test results. The load level is H-M. The components that may be protected and/or attacked at $t = 9, t = 8$ and 9, and $t = 7, 8$, and 9 are removed from search spaces in turn. 42.33% time is saved with only 3.45% error when No. of D = 1, and the set of excluded time is {9}. The error rises gradually when No. of D increases. The error rises sharply if too many time steps are excluded. Thus, system planners are recommended to reduce search spaces properly to balance the computation time and accuracy. This shrinking strategy is intuitive and needs to be further studied.

TABLE XII
COMPARISON BETWEEN ACCURATE AND APPROXIMATE SOLUTIONS

No. of D	Time excluded	System cost (*10^5 $)		Error (%)	Time (s)	
		DAD	DAD‡		DAD	DAD‡
0	{9}	47.942	45.436	5.23	373	212
	{8, 9}		43.601	9.05		73
	{7, 8, 9}		38.692	19.29		38
1	{9}	29.766	28.739	3.45	326	188
	{8, 9}		26.460	11.11		63
	{7, 8, 9}		22.954	22.89		37
2	{9}	13.374	11.690	12.59	409	280
	{8, 9}		9.930	25.75		150
	{7, 8, 9}		4.364	67.37		70
3	{9}	11.123	9.684	12.94	557	329
	{8, 9}		7.857	29.36		211
	{7, 8, 9}		1.457	86.90		43

VI. CONCLUSION

This paper proposes a multi-period RO model to enhance the resilience of the IEGS against SEWEs. Before the hurricane, preventive measures, hardening, are taken in advance to protect the critical components. During the unfolding process, system re-dispatch decisions are made after each hurricane strike to minimize the maximized system cost caused by the hurricane. According to historical or forecast hurricane data, the Markov property is used to construct a data-based (less conservative) uncertainty set by excluding redundant scenarios. The nested C&CG algorithm is adopted to solve the proposed RO model. According to test results, we conclude: i) the reflection point is helpful for system planners to balance the investment cost and the system cost. However, incorporating the investment cost into the objective function may prevent system planners from the most critical components and result in myopic preventive measures; ii) the proposed data-based uncertainty set reduces the conservativeness of the proposed RO model. Besides, it also contributes to the improvement in computational efficiency; iii) although the shrinking strategy is unripe, it shows the potential to reduce the computation time and obtain a high-quality approximate solution. Future work includes: i) improving assumption 3) by introducing failure probability to protected and attacked components; ii) reducing the conservativeness of the RO model by other data-based methods; iii) designing a shrinking strategy to obtain a high-quality approximate solution.

REFERENCES

[1] Q. Wang, X. Chen, A. N. Jha, and H. Rogers, "Natural gas from shale formation—The evolution, evidences and challenges of shale gas revolution in United States," *Renew. Sustain. Energy Rev.*, vol. 30, no. 2, pp. 1–28, Feb. 2014.

[2] *Annual Energy Review*, U.S. Energy Inf. Admin., Washington, DC, USA, 2019. [Online]. Available: https://www.eia.gov/totalenergy/data/annual

[3] *Electricity Generation, Trade and Consumption*, Nat. Stat., London, U.K., 2019. [Online]. Available: https://www.gov.uk/government/statistics/electricity-section-5-energy-trends

[4] C. M. Correa-Posada and P. Sánchez-Martın, "Security-constrained optimal power and natural-gas flow," *IEEE Trans. Power Syst.*, vol. 29, no. 4, pp. 1780–1787, Jul. 2014.

[5] Y. Zhang, Y. Hu, J. Ma, and Z. Bie, "A mixed-integer linear programming approach to security-constrained co-optimization expansion planning of natural gas and electricity transmission systems," *IEEE Trans. Power Syst.*, vol. 33, no. 6, pp. 6368–6378, Nov. 2018.

[6] S. Chen, Z. Wei, G. Sun, W. Wei, and D. Wang, "Convex hull based robust security region for electricity-gas integrated energy systems," *IEEE Trans. Power Syst.*, vol. 34, no. 3, pp. 1740–1748, May 2019.

[7] X. Zhang, L. Che, M. Shahidehpour, A. S. Alabdulwahab, and A. Abusorrah, "Reliability-based optimal planning of electricity and natural gas interconnections for multiple energy hubs," *IEEE Trans. Smart Grid*, vol. 8, no. 4, pp. 1658–1667, Jul. 2017.

[8] C. He, L. Wu, T. Liu, and Z. Bie, "Robust co-optimization planning of interdependent electricity and natural gas systems with a joint N-1 and probabilistic reliability criterion," *IEEE Trans. Power Syst.*, vol. 33, no. 2, pp. 2140–2154, Mar. 2018.

[9] M. Bao, Y. Ding, C. Singh, and C. Shao, "A multi-state model for reliability assessment of integrated gas and power systems utilizing universal generating function techniques," *IEEE Trans. Smart Grid*, vol. 10, no. 6, pp. 6271–6283, Nov. 2019.

[10] Y. He, M. Shahidehpour, Z. Li, C. Guo, and B. Zhu, "Robust constrained operation of integrated electricity-natural gas system considering distributed natural gas storage," *IEEE Trans. Sustain. Energy*, vol. 9, no. 3, pp. 1061–1071, Jul. 2018.

[11] *Economic Benefits of Increasing Electric Grid Resilience to Weather Outages*, Executive Office President. U.S.A., Washington, DC, USA, Aug. 2013. [Online]. Available: http://energy.gov/downloads/economic-benefits-increasing-electric-grid-resilience-weather-outages

[12] *Comparing the Impacts of Northeast Hurricanes on Energy Infrastructure*, Dept. Energy, Washington, DC, USA, 2013. [Online]. Available: https://energy.gov/oe/downloads/comparing-impacts-northeast-hurricanes-energy-infrastructure-april-2013

[13] National Research Council, *Enhancing the Robustness and Resilience of Future Electrical Transmission and Distribution in the United States to Terrorist Attack*. Washington, DC, USA: Nat. Academies Press, 2012.

[14] National Academy of Sciences U.S.A, *National Research Council: Disaster Resilience: A National Imperative*. Washington, DC, USA: Nat. Acad. Press. 2012.

[15] B. Zhao, A. J. Conejo, and R. Sioshansi, "Coordinated expansion planning of natural gas and electric power systems," *IEEE Trans. Power Syst.*, vol. 33, no. 3, pp. 3064–3075, May 2018.

[16] C. Shao, M. Shahidehpour, X. Wang, X. Wang, and B. Wang, "Integrated planning of electricity and natural gas transportation systems for enhancing the power grid resilience," *IEEE Trans. Power Syst.*, vol. 32, no. 6, pp. 4418–4429, Nov. 2017.

[17] L. Wu, C. He, C. Dai, and T. Liu, "Robust network hardening strategy for enhancing resilience of integrated electricity and natural gas distribution systems against natural disasters," *IEEE Trans. Power Syst.*, vol. 33, no. 5, pp. 5787–5798, Sep. 2018.

[18] C. Wang *et al.*, "Robust defense strategy for gas–electric systems against malicious attacks," *IEEE Trans. Power Syst.*, vol. 32, no. 4, pp. 2953–2965, Jul. 2017.

[19] M. H. Amirioun, F. Aminifar, and M. Shahidehpour, "Resilience-promoting proactive scheduling against Hurricanes in multiple energy carrier microgrids," *IEEE Trans. Power Syst.*, vol. 34, no. 3, pp. 2160–2168, May 2019.

[20] S. Lei, J. Wang, C. Chen, and Y. Hou, "Mobile emergency generator pre-positioning and real-time allocation for resilient response to natural disasters," *IEEE Trans. Smart Grid*, vol. 9, no. 3, pp. 2030–2041, May 2018.

[21] M. Yan, Y. He, M. Shahidehpour, X. Ai, Z. Li, and J. Wen, "Coordinated regional-district operation of integrated energy systems for resilience enhancement in natural disasters," *IEEE Trans. Smart Grid*, vol. 10, no. 5, pp. 4881–4892, Sep. 2019.

[22] Y. Li, Z. Li, F. Wen, and M. Shahidehpour, "Minimax-regret robust co-optimization for enhancing the resilience of integrated power distribution and natural gas systems," *IEEE Trans. Sustain. Energy*, vol. 11, no. 1, pp. 61–71, Jan. 2020.

[23] Y. Wang, C. Chen, J. Wang, and R. Baldick, "Research on resilience of power systems under natural disasters—A review," *IEEE Trans. Power Syst.*, vol. 31, no. 2, pp. 1604–1613, Mar. 2016.

[24] J. Li, X. Y. Ma, C. C. Liu, and K. P. Schneider, "Distribution system restoration with microgrids using spanning tree search," *IEEE Trans. Power Syst.*, vol. 29, no. 6, pp. 3021–3029, Nov. 2014.

[25] C. Chen, J. Wang, F. Qiu, and D. Zhao, "Resilient distribution system by microgrids formation after disastrous events," *IEEE Trans. Smart Grid*, vol. 7, no. 2, pp. 958–966, Mar. 2016.

[26] C. P. Nguyen and A. J. Flueck, "Agent based restoration with distributed energy storage support in smart grids," *IEEE Trans. Smart Grid*, vol. 3, no. 2, pp. 1029–1038, Jun. 2012.

[27] Y. Lin, B. Chen, J. Wang, and Z. Bie, "A combined repair crew dispatch problem for resilient electric and natural gas system considering reconfiguration and DG islanding," *IEEE Trans. Power Syst.*, vol. 34, no. 4, pp. 2755–2767, Jul. 2019.
[28] C. Wang, Y. Hou, F. Qiu, S. Lei, and K. Liu, "Resilience enhancement with sequentially proactive operation strategies," *IEEE Trans. Power Syst.*, vol. 32, no. 4, pp. 2847–2857, Jul. 2017.
[29] W. Yuan, J. Wang, F. Qiu, C. Kang, and B. Zeng, "Robust optimization-based resilient distribution network planning against natural disasters," *IEEE Trans. Smart Grid*, vol. 7, no. 6, pp. 2817–2826, Nov. 2016.
[30] Z. Wang and J. Wang, "Self-healing resilient distribution systems based on sectionalization into microgrids," *IEEE Trans. Power Syst.*, vol. 30, no. 6, pp. 3139–3149, Nov. 2015.
[31] (Apr. 2017). *National Hurricane Center*. [Online]. Available: https://www.nhc.noaa.gov/verification
[32] *Hurricane Research Division*. Accessed: Dec. 2018. [Online]. Available: https://www.aoml.noaa.gov/hrd/
[33] *Hurricanes: Science and Society*. Accessed: Oct. 2018. [Online]. Available: http://www.hurricanescience.org
[34] C. M. Correa-Posada, and P. Sanchez-Martin. (2014). *Gas Network Optimization: A Comparison of Piecewise Linear Models*. [Online]. Available: http://www.optimization-online.org/DB_HTML/2014/10/4580.html
[35] D. Bertsimas, E. Litvinov, X. A. Sun, J. Zhao, and T. Zheng, "Adaptive robust optimization for the security constrained unit commitment problem," *IEEE Trans. Power Syst.*, vol. 28, no. 1, pp. 52–63, Feb. 2013.
[36] L. Zhao and B. Zeng. (2012). *An Exact Algorithm for Two-Stage Robust Optimization with Mixed Integer Recourse Problems*. [Online]. Available: http://www.optimization-online.org/DB_FILE/2012/01/3310.pdf
[37] S. Manshadi and M. Khodayar, "Resilient operation of multiple energy carrier microgrids," *IEEE Trans. Smart Grid*, vol. 6, no. 5, pp. 2283–2292, Sep. 2015.

Rong-Peng Liu (Graduate Student Member, IEEE) received the B.E. degree in electrical engineering from Shandong University, Jinan, China, in 2014, and the M.E. degree in electrical engineering from Tianjin University, Tianjin, China, in 2017. He is currently pursuing the Ph.D. degree in electrical and electronic engineering with the University of Hong Kong, Hong Kong. His research interests include the integrated electricity and natural gas systems (IEGS), system resilience, and applications of optimization methods in the IEGS.

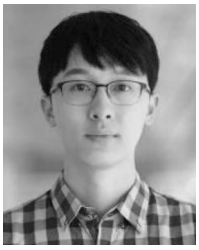

Shunbo Lei (Member, IEEE) received the B.E. degree in electrical engineering from Huazhong University of Science and Technology, Wuhan, China, in 2013, and the Ph.D. degree in electrical engineering from the University of Hong Kong, Hong Kong, in 2017. He was a Visiting Scholar with Argonne National Laboratory, Lemont, IL, USA, from 2015 to 2017. He was a Postdoctoral Researcher with the University of Hong Kong from 2017 to 2019. He is currently a Research Fellow with the University of Michigan, Ann Arbor, MI, USA. His research interests include power system operation, demand response, building energy efficiency, network resilience, convex optimization, and machine learning.

Chaoyi Peng (Member, IEEE) received the B.E. degree in electrical engineering from the Huazhong University of Science and Technology in 2012, and the Ph.D. degree in electrical engineering from the University of Hong Kong in 2016. He was a Postdoctoral Research Fellow with the University of Hong Kong from 2016 to 2018. He joined the Power Dispatch and Control Center of China Southern Power Grid in 2018, where he is currently a Senior Engineer. His research interests include electricity market design and optimization, renewables integration, and big data analytics in power system operation.

Wei Sun (Member, IEEE) received the Ph.D. degree in electrical engineering from Iowa State University, Ames, IA, USA, in 2011. He is currently an Associate Professor with the Department of Electrical and Computer Engineering, University of Central Florida, Orlando, FL, USA. His research interests include power system restoration and self-healing, and cyber-physical security and resilience.

Yunhe Hou (Senior Member, IEEE) received the B.E. and Ph.D. degrees in electrical engineering from the Huazhong University of Science and Technology, Wuhan, China, in 1999 and 2005, respectively. He was a Postdoctoral Research Fellow with Tsinghua University, Beijing, China, from 2005 to 2007, and a Postdoctoral Researcher with Iowa State University, Ames, IA, USA, and the University College Dublin, Dublin, Ireland, from 2008 to 2009. He was also a Visiting Scientist with the Laboratory for Information and Decision Systems, Massachusetts Institute of Technology, Cambridge, MA, USA, in 2010. He has been a Guest Professor with the Huazhong University of Science and Technology since 2017, and an Adviser of China Electric Power Research Institute since 2019. He joined the faculty of the University of Hong Kong, Hong Kong, in 2009, where he is currently an Associate Professor with the Department of Electrical and Electronic Engineering. He is an Editor of the IEEE TRANSACTIONS ON SMART GRID and an Associate Editor of the *Journal of Modern Power Systems and Clean Energy*.